

Size and Charge Effects on the Binding of CO to Small Isolated Rhodium Clusters<sup>†</sup>André Fielicke,<sup>‡</sup> Gert von Helden,<sup>§</sup> Gerard Meijer,<sup>§</sup> David B. Pedersen,<sup>||</sup> Benoit Simard,<sup>||</sup> and David M. Rayner<sup>\*||</sup>

FOM-Institute for Plasma Physics Rijnhuizen, Edisonbaan 14, NL-3439 MN Nieuwegein, The Netherlands, Fritz-Haber-Institut der Max-Planck-Gesellschaft, Faradayweg 4-6, D-14195 Berlin, Germany, and Steacie Institute for Molecular Sciences, National Research Council, 100 Sussex Drive, Ottawa, Ontario K1A 0R6, Canada

Received: February 20, 2004; In Final Form: April 20, 2004

The adsorption of carbon monoxide on rhodium clusters in the size range of 3–15 atoms is studied in the gas phase using the frequency of the internal CO stretch,  $\nu(\text{CO})$ , to probe the bonding situation of the CO. The IR absorption spectra of neutral, cationic, and anionic  $\text{Rh}_n\text{CO}$  complexes are measured in the frequency range of  $\nu(\text{CO})$ , between 1650 and 2200  $\text{cm}^{-1}$ , using IR multiple photon dissociation spectroscopy. We find that for most clusters adsorption in an atop position ( $\mu^1$ ) is preferred; however, for some clusters, CO in bridging ( $\mu^2$ ) or hollow ( $\mu^3$ ) sites can be identified as well. Comparison with DFT calculations carried out for the smallest cluster complexes  $\text{Rh}_n\text{CO}^{+/0/-}$  ( $n = 3$  and 4) shows that the experimentally identified CO adsorption sites correspond to the energetically favored positions.

## I. Introduction

Carbon monoxide has long been used to probe transition metal atoms and small clusters adsorbed to supports as potential or model catalysts. A pedagogical system has been rhodium adsorbed on metal oxides. Already in early studies of rhodium dispersed on amorphous metal oxide supports,<sup>1,2</sup> the infrared (IR) spectroscopy of adsorbed CO has been used to characterize binding sites and cluster–support interactions. The approach takes advantage of the high sensitivity of the CO stretching frequency,  $\nu(\text{CO})$ , to structure and electron density at the binding site.

Exactly how  $\nu(\text{CO})$  is sensitive to binding site geometry and charge density is of increasing relevance as CO is used in conjunction with methods to investigate deposited clusters of known size that are currently being deployed to investigate model catalysts. Such techniques include size-selective deposition<sup>2</sup> and postdeposition characterization by scanning probe microscopy.<sup>3–5</sup> Until recently, the interpretation of the vibrational spectroscopy of CO adsorbed on supported metal species relied on comparison with  $\nu(\text{CO})$  values of stable, molecular metal carbonyl compounds, of CO adsorbed on single-crystal surfaces, and of atom–CO complexes in rare gas matrixes.

Gas-phase studies of isolated metal cluster–carbonyl complexes provide a more secure foundation for interpreting CO probes of supported clusters. The effects of structure, size, and charge on the binding of CO to the clusters are reflected in the  $\nu(\text{CO})$  frequencies and, therefore, those values provide a baseline to identify and quantify support effects. For instance, how  $\nu(\text{CO})$  for a particular binding configuration and for a particular cluster size varies with the charge on the cluster provides an assessment of the amount of charge transferred to the support. This approach

has previously been limited to using  $\nu(\text{CO})$  measured in low-temperature matrixes for the neutral, anionic, and cationic atom–CO,  $\text{RhCO}$ , complexes.<sup>6,7</sup> The equivalent information has not been obtained for unsaturated cluster complexes.

Recently we began to address this problem, extending the technique of IR multiple-photon dissociation (IRMPD) spectroscopy to investigate rhodium cluster–CO complexes,  $\text{Rh}_n\text{CO}$ , in the gas phase. The experiments take advantage of the tunable, intense IR radiation from the Free Electron Laser for Infrared eXperiments (FELIX), which is well suited for the IRMPD spectroscopy of cluster–ligand complexes.<sup>8</sup> We have already communicated results for the neutral species  $\text{Rh}_n\text{CO}$  ( $n = 6–20$ ).<sup>9</sup> We found that CO binds almost exclusively in an atop ( $\mu^1$ ) configuration. The exception was  $\text{Rh}_{12}\text{CO}$ , where there was inconclusive evidence for a coexisting bridge-bound ( $\mu^2$ ) species. Reported values for supported clusters show shifts in  $\nu(\text{CO})$  of as much as +100  $\text{cm}^{-1}$  relative to our findings for the free clusters. Significant charge transfer to the support was indicated but could not be quantified because the experiments were only performed on neutral clusters. In addition, there was limited comparison with existing theory because we did not obtain spectra for clusters with  $n < 6$  in our initial study.<sup>9</sup>

Experimental developments now let us access smaller anionic and cationic as well as neutral clusters. Here, we report the IR spectra in the CO stretching region for  $\text{Rh}_n\text{CO}^{+/0/-}$  ( $n = 3–15$ ). We find that CO binds preferentially at sites involving more than one metal atom on the smaller clusters with  $n = 3$  and 4. The experimental data are complemented by DFT calculations. The experimentally identified CO adsorption sites correspond also to the energetically favored positions found by our calculations. Improved signal-to-noise ratios also allow us to confirm that CO can bind to  $\text{Rh}_{12}\text{CO}$  in either  $\mu^1$  or  $\mu^2$  geometries and to identify a limited number of other clusters that exhibit some degree of binding at bridge or hollow sites.

## II. Experimental Methods

The experiments are performed in a molecular beam apparatus coupled to the beam line of the FELIX.<sup>10,11</sup> This setup, as used

<sup>†</sup> Part of the special issue “Gerhard Ertl Festschrift”.

\* To whom correspondence should be addressed. E-mail: David.Rayner@nrc-cnrc.gc.ca.

<sup>‡</sup> FOM-Institute for Plasma Physics Rijnhuizen.

<sup>§</sup> Fritz-Haber-Institut der Max-Planck-Gesellschaft.

<sup>||</sup> Steacie Institute for Molecular Sciences.

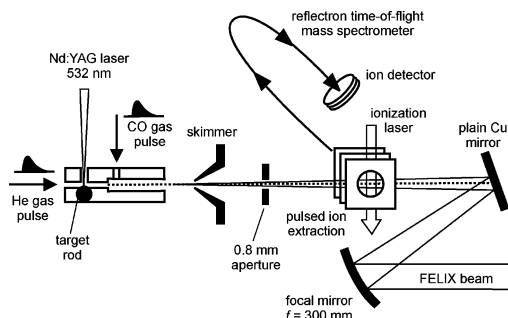


**Figure 1.** Scheme of the experimental setup for IR multiple photon dissociation spectroscopy on metal cluster complexes. The flight path of the clusters is indicated by a dashed line. Neutral clusters are ionized with an  $F_2$  laser (157 nm,  $\sim 0.5$  mJ/pulse).

for IR spectroscopy of metal clusters, metal compound clusters, and cluster–ligand complexes, has been described in parts earlier.<sup>9,11,12</sup> Here we give a detailed description of the IR-MPD experiments on metal cluster complexes. Figure 1 shows a scheme of the experimental setup.

Clusters are produced in a pulsed laser vaporization source by ablating the material from a rhodium rod using the 2nd harmonic output of a Nd:YAG laser ( $\sim 10$  mJ/pulse) in a 3 mm diameter clustering channel in the presence of a short pulse of helium delivered by a current-loop actuated valve (R. M. Jordan Company, Inc.). Neutral, cationic, and anionic metal clusters are formed in this process. Reactions with CO are initiated by injecting a short gas pulse of CO via a second pulsed valve (General Valve, Series 9) into a 5 mm diameter, 35 mm long cluster flow-reactor channel that starts 30 mm downstream from the laser vaporization region. We have not characterized the cluster beam temperature by direct measurement but, due to the pressure of several tens of mbar in the clustering channel, we expect that the clusters thermalize rapidly and enter the reactor at near 300 K thermal energies. Where the beam temperature of transition metal cluster sources with similar dimensions and flow characteristics has been established independently, it has been shown that the clusters are thermalized at the source temperature.<sup>13–15</sup> These studies also confirm that under the prevailing mild expansion conditions there is no significant additional cooling in the supersonic expansion. On exiting the reactor, the reaction mixture expands into vacuum and forms a molecular beam, and further bimolecular reactions are effectively stopped. The molecular beam is shaped with a skimmer followed by an aperture of 0.8 mm diameter. Deflection plates between the skimmer and aperture are used to remove ionic species from the beam when neutral species are studied. The distribution of the clusters and their complexes with CO is analyzed with a reflectron time-of-flight mass spectrometer (R. M. Jordan Company, Inc.) using pulsed acceleration voltages. Ion extraction is orthogonal to the cluster beam direction. Neutral species are ionized between the extraction plates of the mass spectrometer using a pulsed nanosecond excimer laser (PSX100, NEWKES SE) run on  $F_2$  (157 nm, 7.9 eV, 5 ns,  $\sim 0.5$  mJ/pulse) or ArF (193 nm, 6.4 eV, 5 ns,  $\sim 3.5$  mJ/pulse). Although the UV light is slightly focused, the laser fluence is kept sufficiently low to avoid fragmentation induced by absorption of multiple UV photons. For the detection of the anions, all voltages of the mass spectrometer are reversed.

For obtaining IR spectra, the molecular beam is longitudinally overlapped with the pulsed IR laser beam of FELIX. The IR beam is focused through the 0.8 mm aperture to ensure that the cluster beam entering the mass spectrometer is completely irradiated. If the IR light is resonant with an IR active mode of

the cluster complex one or more photons can be absorbed. In principle, absorption can be followed by different cooling mechanisms such as radiation, electron emission, or fragmentation. Electron emission and fragmentation both lead to changes in the cluster distribution that can be probed using mass spectrometry. For the systems we are studying here, fragmentation involving loss of the CO ligands is observed to be the dominant cooling process. The ions are extracted  $\sim 50$   $\mu$ s after the FELIX pulse meaning that fragmentation is observed if the dissociation rate is greater than  $\sim 2 \times 10^4$   $s^{-1}$ . Depletion of the mass spectrometric signal of a cluster complex is always accompanied with growth of the signal of a corresponding fragment. The cluster source is operated at 10 Hz, whereas FELIX runs at a 5 Hz repetition rate. Relative intensities of the cluster complexes, observed in the presence and absence of FELIX irradiation, are calculated from the alternately recorded mass spectra. This procedure compensates for drifts in the output of the cluster source over the acquisition time (source stability is a limiting factor in depletion experiments). To compensate for the pulse-to-pulse fluctuations, that can be as large as 50%, we typically average over 300 shots per wavelength point. The IR spectra are constructed by plotting the relative intensity of the integrated mass spectrometric signal of a species as a function of the wavelength of FELIX.

The light output of FELIX consists of macro pulses of typically 5  $\mu$ s duration that have a temporal sub structure with micro pulses of  $\sim 2$  ps duration and spaced by 1 ns. For the spectroscopy on the rhodium cluster carbonyls, we used FELIX macro pulse energies of typically 10 mJ. The IR wavelength is calibrated by recording the IR absorption spectrum of ethene on the  $\nu_7 + \nu_8$  combination band in a photo acoustic cell. From this, we estimate that we achieve an absolute accuracy of our wavenumber scale of  $\pm 2$   $cm^{-1}$  around 2000  $cm^{-1}$ . By measuring the width of the Q-branch of the  $\nu_7 + \nu_8$  transition of ethene, the spectral bandwidth of FELIX is found to be 10–20  $cm^{-1}$  at 1890  $cm^{-1}$ , in agreement with a Fourier transform limited bandwidth of the pulsed laser radiation.

### III. Computational Methods

We perform density functional theory (DFT) calculations on rhodium cluster carbonyls with the B3PW91 functional and the LACV3P\* basis set using the Jaguar 4.0 program.<sup>16</sup> Earlier calculations have shown that by using B3PW91 one obtains the correct  $^4F$  ground state for the Rh atom.<sup>17</sup> With the nonhybrid functional PW91, we find the  $^2D$  state to be the energetically lowest. The LACV3P\* basis set uses Pople's 6–331G\* basis<sup>18</sup> for C and O and a triple- $\zeta$ -valence contraction of the original Hay-Wadt effective core potential basis set<sup>19</sup> implemented in Jaguar 4.0. For the calculations on the anionic clusters, we use diffuse functions (5 d). We also use diffuse functions on CO in calculating the binding energies of the anionic complexes. Relative energies are given without any additional corrections. Geometry optimizations were unrestricted for both the bare clusters and the CO complexes. CO binding did not alter the metal cluster structure apart from slight changes in bond lengths. We calculated the harmonic vibrational frequencies and the corresponding IR intensities numerically.

We tested the reliability of the theoretical method by using it to predict the relative energies and vibrational frequencies of the neutral and charged Rh atom and Rh–CO complexes (Tables 1 and 2). It is found that both the electron binding energy and the ionization potential of the Rh atom are accurately calculated. All tabulated calculated frequencies are scaled with a constant factor of 0.9588 as this is the ratio of the experimental to the

**TABLE 1: Calculated Relative Energies (in eV) of Different Charge States of Rh Using the B3PW91 Functional and the LACV3P\* Basis Set, Compared to Experimental Values**

	electronic state	rel. energy (eV)	exp. value (eV)
Rh <sup>+</sup>	<sup>3</sup> F (d <sup>8</sup> s <sup>0</sup> )	+7.60	+7.46 <sup>a</sup>
Rh	<sup>4</sup> F (d <sup>8</sup> s <sup>1</sup> )	0	
Rh <sup>-</sup>	<sup>2</sup> D (d <sup>9</sup> s <sup>0</sup> )	+0.29	+0.41 <sup>b</sup>
	<sup>3</sup> F (d <sup>8</sup> s <sup>2</sup> )	-1.12	-1.13 <sup>c</sup>

<sup>a</sup> First ionization potential of Rh atom.<sup>35</sup> <sup>b</sup> Reference 36. <sup>c</sup> Electron affinity of Rh atom.<sup>37</sup>

calculated value for the internal stretch frequency of the free CO molecule. The  $\nu(\text{CO})$  values obtained in this manner for neutral and charged Rh–CO (Table 2) are in good agreement with the experimental data of Zhou et al.<sup>6,7</sup> Here it should be remarked that those data have been measured using matrix isolation spectroscopy, and the matrix effect could lead to modest frequency shifts.

#### IV. Results and Discussion

**Mass Spectra.** Figure 2 shows parts of typical mass spectra obtained for cationic, neutral, and anionic rhodium clusters and their CO complexes. The opening time and the backing pressure of the second pulsed valve are adjusted to yield mainly cluster complexes with one CO molecule attached. We have not quantified the reactivity of the clusters to CO; however, we observe that to form the complexes of the neutral clusters  $\sim 10$  times higher CO backing pressures are necessary than for the ionic clusters. Bimolecular absolute rate constants for the CO adsorption on rhodium cluster cations and anions have been published recently<sup>20</sup> showing an onset of the reactivity around Rh<sub>4</sub><sup>+/-</sup>.

In the IRMPD experiments on neutral clusters presented here, the clusters are ionized with an F<sub>2</sub> laser (7.9 eV/photon). This allows us to ionize small cluster carbonyls Rh<sub>n</sub>CO ( $n = 3-5$ ) that we were not able to ionize in our earlier experiments using an ArF excimer laser (6.4 eV/photon).<sup>9</sup> Also the bare clusters Rh<sub>3</sub> and Rh<sub>4</sub> are hardly ionized with the unfocused ArF excimer laser, and it appears therefore that the IPs of Rh<sub>3</sub> and Rh<sub>4</sub> lie between 6.4 and 7.9 eV.

**Infrared Spectra.** The IR MPD-spectra for Rh<sub>n</sub>CO<sup>+0/-</sup> species in the size range of  $n = 3-15$  are shown in Figure 3. In addition to these overview spectra, the spectral ranges around the observed transitions have been scanned with higher resolution and lower FELIX intensity to obtain sharper/narrower absorption bands. Experimental values for  $\nu(\text{CO})$  extracted from these spectra are listed in Table 3. The bands can be assigned on the basis of what is known about  $\nu(\text{CO})$  for CO at different binding geometries on metal surfaces, in conjunction with the charge-induced shifts measured for RhCO<sup>+0/-</sup> species in matrices<sup>6,7</sup> and our DFT calculations on Rh<sub>n</sub>CO<sup>+0/-</sup> ( $n = 3$  and 4), vide infra. We identify the type of binding site from

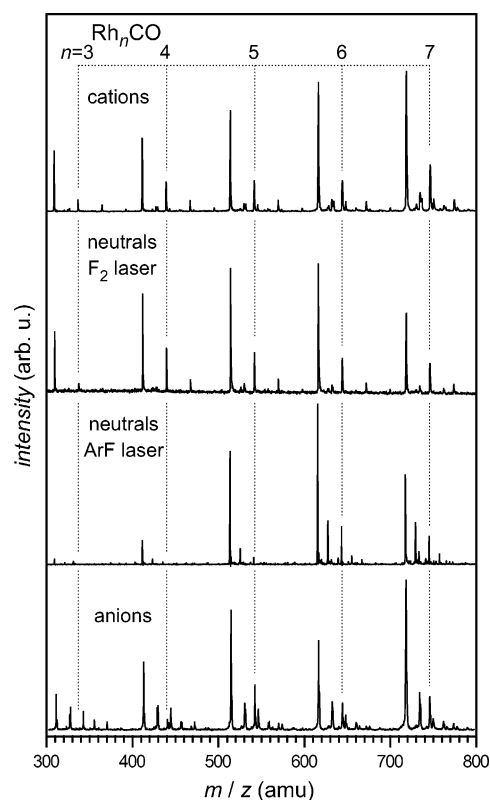


**Figure 2.** Mass spectra of neutral and charged Rh<sub>n</sub>CO species in the range of Rh<sub>3</sub>–Rh<sub>7</sub>. The cationic and anionic clusters are emitted directly from the cluster source. The neutral clusters are ionized with an ArF laser (193 nm, 6.4 eV) or with an F<sub>2</sub> laser (157 nm, 7.9 eV). Additional peaks in the spectra are mainly due to contaminations by carbides and oxides.

$\nu(\text{CO})$ , taking the shifts due to charge into account. For the cations, we find  $\mu^1$  species that absorb in the range 2010–2054 cm<sup>-1</sup>,  $\mu^2$  species that absorb in the range 1887–1903 cm<sup>-1</sup>, and a  $\mu^3$  species that absorbs at 1788 cm<sup>-1</sup>. In the case of the neutrals, we find absorption in the range 1949–1964 cm<sup>-1</sup> for  $\mu^1$  species, in the range 1810–1838 cm<sup>-1</sup> for  $\mu^2$ , and at 1731 cm<sup>-1</sup> for a  $\mu^3$  species. For the anions, the ranges are 1847–1905 cm<sup>-1</sup> for the  $\mu^1$  species and 1720–1767 cm<sup>-1</sup> for the  $\mu^2$  species. The atom–complex results, see Table 2, provide limits for the charge-induced shifts. These shifts are expected to decrease as the cluster size increases due to charge dilution, and indeed, this is what we observe (Figure 4) and what we find for Rh<sub>n</sub>CO<sup>+0/-</sup> ( $n = 3$  and 4) from DFT. The decrease is gradual, and up to the biggest clusters investigated here, the values for the neutral cluster are not reached. A detailed discussion and a model for this size-dependent shift will be given elsewhere.

Looking at bridged versus atop bonding, the predominant form of binding is atop for all three charge states. Clusters with

**TABLE 2: Calculated Energies, Bond Lengths, Vibrational Frequencies, and IR Intensities for Neutral and Charged Rh–CO Species**

	rel. energy (eV)	CO binding energy (eV)	$d(\text{C}-\text{O})^a$ $d(\text{M}-\text{C})$ (pm)	$\nu(\text{CO})$ $\nu(\text{M}-\text{C})$ (cm <sup>-1</sup> )	IR intensities (km/mol <sup>-1</sup> )	$\nu(\text{CO})$ exp. (cm <sup>-1</sup> ) <sup>b</sup>
RhCO <sup>+</sup> ( <sup>3</sup> Δ)	+7.89	2.08	112.2 195.4	2174.7 354.6	258.4 8.0	2174.1
RhCO ( <sup>2</sup> Δ)	0	2.38	114.7 182.9	2025.7 504.5	619.5 6.5	2022.5
RhCO <sup>-</sup> ( <sup>1</sup> Σ <sup>+</sup> )	-1.38	2.56	118.2 174.0	1829.0 586.6	1123.8 1.2	1828.6

<sup>a</sup> Calculated bond length of free CO is 112.7 pm. <sup>b</sup> Measured in a Ne matrix.<sup>7,6</sup>

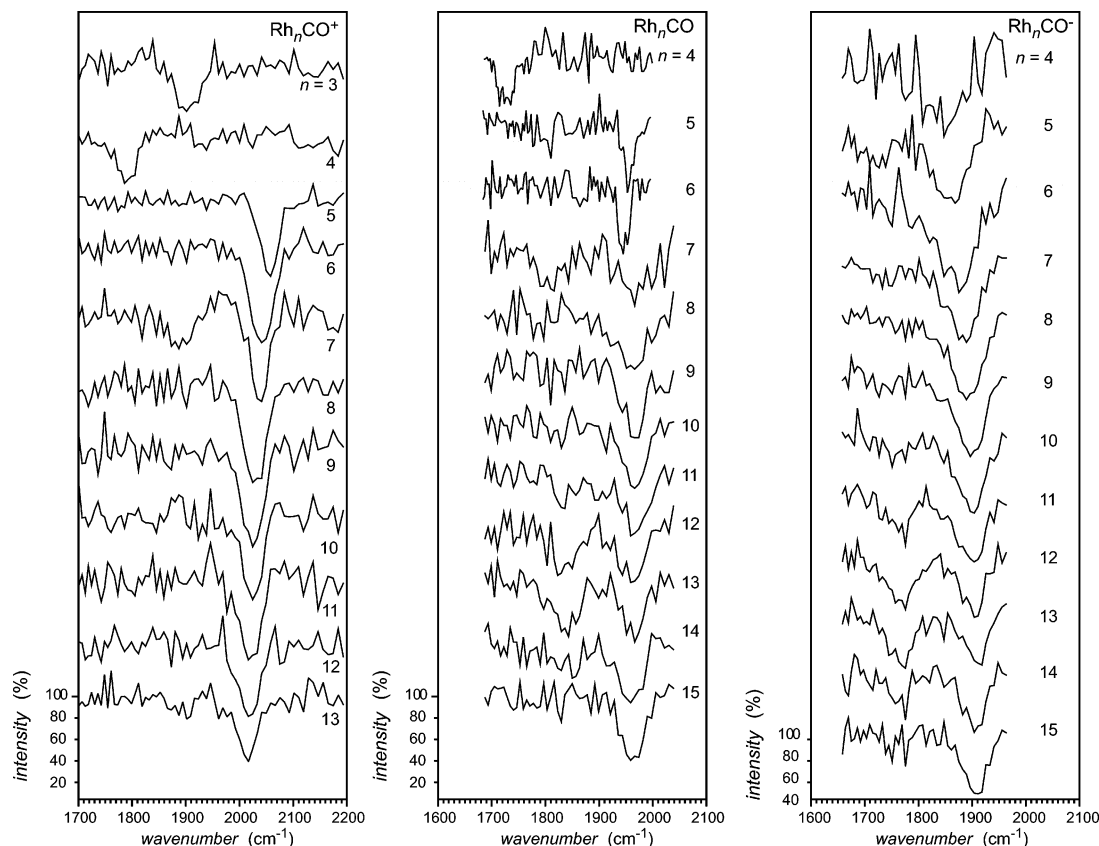


**Figure 3.** IR-MPD spectra of  $\text{Rh}_n\text{CO}^{+0/-}$  complexes in the spectral region around  $\nu(\text{CO})$ . The relative intensity (in percent) of the ion signal is plotted versus the IR frequency. The spectra of the smaller neutral cluster complexes have been measured separately, under slightly different experimental conditions.

**TABLE 3: Experimental IR Stretch Frequencies  $\nu(\text{CO})$  (in  $\text{cm}^{-1}$ ) for Rhodium Cluster Mono Carbonyls  $\text{Rh}_n\text{CO}^{0+/-}$**

$n$	cations			neutrals			anions	
	$\mu^1$	$\mu^2$	$\mu^3$	$\mu^1$	$\mu^2$	$\mu^3$	$\mu^1$	$\mu^2$
3		1903						
4			1788			1731	1847	
5	2054			1960			1857	1720
6	2038			1949			1873	
7	2036	1887		1960	1810		1883	
8	2026			1960			1890	
9	2022			1962			1897	
10	2021			1964			1899	
11	2018			1964			1898	1764
12	2016			1964	1836		1901	1767
13	2013			1962	1838		1905	1767
14	2011			1962			1903	1765
15	2010			1959			1905	

$n \geq 5$  always show  $\mu^1$  atop binding. In selected cases,  $\mu^2$  bridging sites are also evident. Bridge binding in the absence of  $\mu^1$  binding is only observed on the small cluster complexes  $\text{Rh}_3\text{CO}^+$ ,  $\text{Rh}_4\text{CO}$ , and  $\text{Rh}_4\text{CO}^+$  (although we do not measure  $\text{Rh}_3\text{CO}$  and  $\text{Rh}_3\text{CO}^-$ ). Hollow site  $\mu^3$  binding is only observed for  $\text{Rh}_4\text{CO}$  and  $\text{Rh}_4\text{CO}^+$ . For the small clusters ( $n = 3$  and 4), full consistency is found between the lowest energy binding site identified by DFT and the type of binding identified by  $\nu(\text{CO})$ .

The presence of more than one  $\nu(\text{CO})$  band in the spectrum of  $\text{Rh}_n(\text{CO})^{+0/-}$  can only be explained by the presence of isomers. These isomers may result from metal cluster isomers or from a single metal cluster isomer exhibiting more than one binding site. For some individual, larger  $\text{Rh}_n\text{CO}^{+0/-}$  complexes, bands corresponding to both  $\mu^1$  and  $\mu^2$  are found. We observe the presence of the two isomeric forms in  $\text{Rh}_7\text{CO}^+$ ,  $\text{Rh}_7\text{CO}$ ,

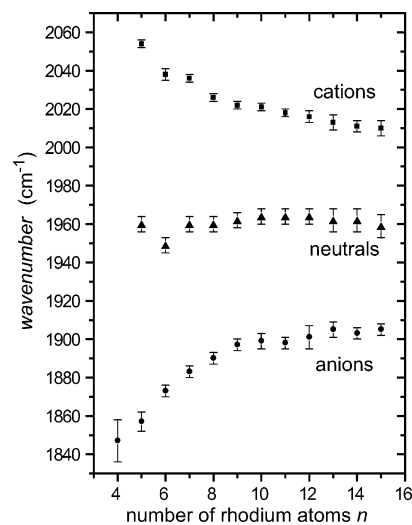


**Figure 4.** Frequency of the  $\nu(\text{CO})$  vibration of atop-CO in  $\text{Rh}_n\text{CO}$  cations ( $\blacksquare$ ), neutrals ( $\blacktriangle$ ), and anions ( $\bullet$ ) as a function of cluster size. The peak positions are determined by a least-squares fit to a Gaussian peak shape. The error bars represent the standard deviation ( $1\sigma$ ) of the fit.

$\text{Rh}_{12}\text{CO}$ ,  $\text{Rh}_{13}\text{CO}$ ,  $\text{Rh}_5\text{CO}^-$ , and  $\text{Rh}_{11-14}\text{CO}^-$ . The relative abundances of the isomeric complexes,  $\mu^1$  and  $\mu^2$ , can be estimated from the amount of depletion in the corresponding absorption bands; the observed amount of depletion gives a lower limit for the abundance of the corresponding isomer directly. For example, for the anionic complex  $\text{Rh}_{10}\text{CO}^-$ , we observe mainly the  $\mu^1$  isomer (60% depletion) and only minor amounts of  $\mu^2$  (15% depletion), for  $\text{Rh}_{11}\text{CO}^-$  the depletions are  $\sim 50\%$  for  $\mu^1$  and  $\sim 30\%$  for  $\mu^2$ . Equal amounts of  $\mu^1$  and  $\mu^2$

**TABLE 4: Calculated CO Binding Energies, Multiplicities of the Electronic Ground States, Vibrational Frequencies, and IR Intensities for Neutral and Charged  $\text{Rh}_n\text{CO}$  ( $n = 3$  and  $4$ ) Complexes<sup>a</sup>**

		CO binding energy (eV)	multiplicity	$\nu(\text{C}-\text{O})$ ( $\text{cm}^{-1}$ )	IR intensity ( $\text{km}/\text{mol}^{-1}$ )	$\nu(\text{C}-\text{O})$ exp. ( $\text{cm}^{-1}$ )	$\nu(\text{M}-\text{C})$ ( $\text{cm}^{-1}$ )	IR intensity ( $\text{km}/\text{mol}^{-1}$ )	
$\text{Rh}_3\text{CO}^+$	$\mu^1$	1.79	3	2065	570.3		533	16.4	
	$\mu^2$	2.18	5	1909	484.3	$1903 \pm 5$	428/480	3.1/8.5	
	$\mu^3$	2.07	5	1822	408.9		343/351/387	1.6/1.3/1.2	
$\text{Rh}_3\text{CO}$	$\mu^1$	2.04	4	1974	713.7			567	5.4
	$\mu^2$	2.28	4	1791	618.6		460/490	1.1/1.3	
	$\mu^3$	2.23	4	1723	453.9		373/377/425	0.5/0.6/0.1	
$\text{Rh}_3\text{CO}^-$	$\mu^1$	2.45	1	1849	1501.3		517	1.3	
	$\mu^2$	2.71	3	1654	820.1		470/583	1.1/0.7	
	$\mu^3$	2.42 <sup>b</sup>	3	1597	559.5		517/399	10.4/2.2	
$\text{Rh}_4\text{CO}^+$	$\mu^1$	1.33	6	2051	779.0		479	20.6	
	$\mu^2$	1.73	6	1863	601.3		448/513	5.3/6.7	
	$\mu^3$	1.84	6	1764	472.3	$1788 \pm 4$	357/389/413	0.6/4.6/3.5	
$\text{Rh}_4\text{CO}$	$\mu^1$	2.32	5	1967	1054.1			494	11.5
	$\mu^2$	2.31	5	1783	744.2			462/515	1.4/0.1
	$\mu^3$	2.52	5	1674	546.8	$1731 \pm 3$	417/436/439	0.7/3.8/2.0	
$\text{Rh}_4\text{CO}^-$	$\mu^1$	2.54	6	1861	1600.9		$1847 \pm 11$	513	4.8
	$\mu^2$	2.45	4	1628	926.9				448/631
	$\mu^3$	2.54	4	1571	697			426/456/457	0.4/0.1/0.1

<sup>a</sup> The values experimentally determined in this work are given as well. Although the  $\mu^1$  structure has only one M–C stretch mode, there are two modes for  $\mu^2$  and three modes for the  $\mu^3$  bound complexes. The lowest frequency  $\nu(\text{M}-\text{C})$  mode corresponds to the symmetric stretch vibration.  
<sup>b</sup> Only a  $\mu^3$ -bound transition state has been found that has  $C_{2v}$  symmetry and that is strongly distorted toward a  $\mu^2$  structure.

are observed for  $\text{Rh}_{13}\text{CO}^-$  ( $\sim 40\%$  and  $\sim 40\%$ ). The total percentage of experimental depletion, summed over all isomers, is at maximum 75–90%. Even for complexes having no isomers, we do not observe total depletion although intensity studies show that we saturate the depletion in many cases. This we attribute to incomplete overlap of the FELIX beam with the molecular beam so that 90% experimental depletion registers full depletion of the cluster complexes that have experienced the full infrared intensity. Our maximum observed depletion is very sensitive to the alignment and focal position of the infrared beam with respect to the aperture used to mask out the cluster complexes that have not been exposed to the FELIX beam.

An alternative is that a portion of the complexes does not dissociate on the time scale of the experiment either because their infrared oscillator strength is exceptionally low or because the CO ligand is exceptionally strongly bound (an extreme case would be if the CO has dissociatively chemisorbed). The infrared oscillator strength is predicted to drop on going from  $\mu^1$  to  $\mu^3$  bonding and the binding energies may also vary (Table 3). The spectra for  $\text{Rh}_{13}\text{CO}$  and  $\text{Rh}_{13}\text{CO}^-$ , where there is substantial absorption credited to the  $\mu^2$  complex and where the overall experimental depletion is close to the limit determined by beam overlap, show that we can saturate complexes with  $\mu^2$  binding. We therefore expect that the ability to detect  $\mu^2$  complexes solely rests on their abundance. Our background noise level varies from 5 to 20%, depending on the complex in question. Inspection of the individual spectra, and consideration of the overall depletion, allows one to estimate the amount of  $\mu^2$  isomers that might be missed due to the background noise. In the two cases where we observe  $\mu^3$  binding,  $\text{Rh}_4\text{CO}^+$  and  $\text{Rh}_4\text{CO}$ , we only reach  $\sim 50\%$  depletion; therefore, it is more likely to miss  $\mu^3$  complexes.

The formation of isomeric  $\text{Rh}_n\text{CO}^{+/0/-}$  complexes having  $\mu^1$  or  $\mu^2$  binding might be due to two reasons: (i) the cluster beam may contain cluster isomers with one (set of) isomer(s) favoring  $\mu^1$  binding and the other  $\mu^2$  binding and (ii) a single cluster structure might exhibit two binding sites. The presence of cluster isomers is well documented in the case of other transition metals.<sup>21</sup> Most of the complexes showing two  $\nu(\text{CO})$  resonances are in the cluster size range of  $n = 11$ –14. This is the size range in which clusters begin to incorporate a central atom and

so-called “inside” and “outside” clusters can coexist over this size range.<sup>22</sup> We expect complex formation to be under thermodynamic control in the reactor resulting in binding at the lowest energy site. We have observed some differences in the amount of  $\mu^2$  binding between runs done on different days. For instance, there is little evidence for  $\mu^2$  binding in  $\text{Rh}_7\text{CO}$  and in  $\text{Rh}_{13}\text{CO}$  in the spectra reported earlier on the neutral complexes.<sup>9</sup> It is reasonable that the isomer composition of the beam is somewhat sensitive to source conditions that can vary from day to day. The observation of isomeric forms may also indicate competitive adsorption at sites with nearly identical binding energies. On the basis of the IR-MPD spectra in the  $\nu(\text{CO})$  range, we cannot decide about the nature of the isomers, i.e., whether they are formed by binding of CO to different sites on one cluster or due to metal cluster isomers.

More structural information could come from the M–C stretching frequency,  $\nu(\text{MC})$ . For instance,  $\mu^3$  binding is expected to result in three distinct frequencies (Table 4). Until now, all of our attempts to measure spectra in the range of the  $\nu(\text{MC})$  stretches have failed; although the IR pulse energy produced by FELIX is about 10 times higher around  $500 \text{ cm}^{-1}$  than at  $\sim 2000 \text{ cm}^{-1}$ , the expected absorption cross-sections for  $\nu(\text{MC})$  are lower than those for  $\nu(\text{CO})$  by more than 2 orders of magnitude.

Our findings can be compared to available data for more saturated cluster carbonyls. IR spectra for the stable cluster carbonyl compounds  $\text{Rh}_4\text{CO}_{12}$  and  $\text{Rh}_6\text{CO}_{16}$  have been known for a long time.<sup>23,24</sup> The vibrations associated with  $\mu^1$  CO stretches are found in the range of 2026–2074  $\text{cm}^{-1}$ .  $\text{Rh}_4\text{CO}_{12}$  contains  $\mu^2$  CO bridges that have the  $\nu(\text{CO})$  absorptions at  $\sim 1885 \text{ cm}^{-1}$ , and in the IR spectrum of  $\text{Rh}_6\text{CO}_{16}$ , the band at  $\sim 1800 \text{ cm}^{-1}$  can be assigned to the  $\mu^3$  bound CO ligands. Both values are higher than what we find for  $\mu^2$  bridges (1810–1838  $\text{cm}^{-1}$ ) and  $\mu^3$  bound CO ( $\text{Rh}_4\text{CO}$ : 1731  $\text{cm}^{-1}$ ) on neutral clusters. The much higher CO content of  $\text{Rh}_4\text{CO}_{12}$  and  $\text{Rh}_6\text{CO}_{16}$  accounts for a reduced strength of the back-bonding to the individual ligands, and therefore, the observed  $\nu(\text{CO})$  bands are closer to the free CO stretch frequency than  $\nu(\text{CO})$  for isolated CO ligands on a cluster surface. In fact, the  $\nu(\text{CO})$  values for  $\text{Rh}_4\text{CO}_{12}$  and  $\text{Rh}_6\text{CO}_{16}$  are close to the frequencies we find for the cationic mono-carbonyl complexes (Table 3).

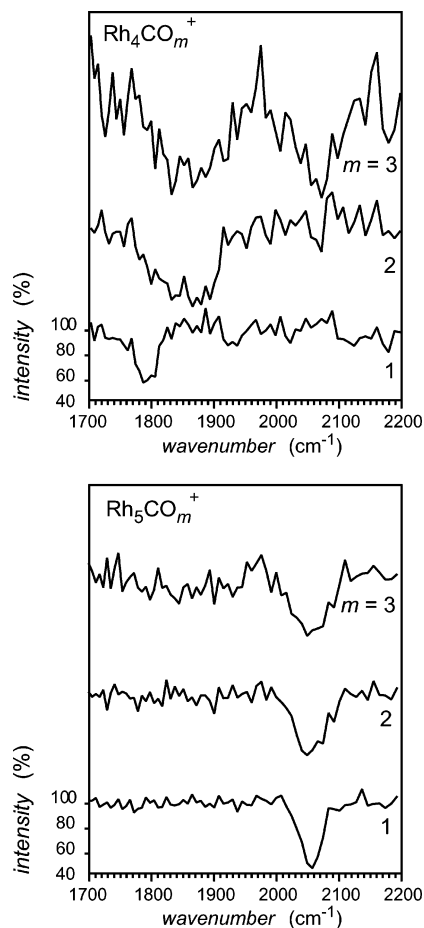


**Figure 5.** IR-MPD spectra of  $\text{Rh}_n(\text{CO})_m^+$  ( $n = 4$  and  $5$ ) complexes in the spectral region of  $\nu(\text{CO})$  for different CO coverages,  $m$ .

By increasing the CO flow, we can produce higher CO coverage on the isolated gas-phase clusters. We limit ourselves here to the discussion of results for  $\text{Rh}_n(\text{CO})_m$  with  $m \leq 3$ . Overlap in the mass spectra, ambiguity introduced by production from higher  $m$  complexes competing with depletion, and signal-to-noise issues limit the amount of information we have obtained so far. The general observation is that for clusters with  $n \geq 5$  addition of further CO ligands up to  $m = 3$  broadens the IR spectrum but does not significantly shift it ( $< 10 \text{ cm}^{-1}$  to the blue). The spectra of  $\text{Rh}_5(\text{CO})_m^+$  ( $m = 1-3$ ) shown in Figure 5 are a typical example in the case of the predominant  $\mu^1$  binding. The complexes that show some degree of  $\mu^2$  binding continue to do so when more CO is added, although it is difficult to tell the nature of the binding site for the 2nd and 3rd ligands. Again there is broadening but no large shifts.

In contrast,  $\text{Rh}_n\text{CO}$  complexes with  $n \leq 4$  can be more sensitive to the addition of further CO. In the case of  $\text{Rh}_4(\text{CO})_m^+$  ( $m = 1-3$ ; Figure 5), the IR spectra show that the addition of a second CO ligand causes occupation of a different type of site or that it causes rearrangement in the complex. The absorption in  $\text{Rh}_4(\text{CO})_2^+$  is shifted substantially to the blue of the relatively narrow peak at  $1788 \text{ cm}^{-1}$  observed for  $\text{Rh}_4\text{CO}^+$ . The new absorption band is broader, is asymmetric, and spans the range between the bands found for  $\mu^2$  binding in monocarbonyl cations ( $\sim 1900 \text{ cm}^{-1}$ ) and the  $\mu^3$  frequency, suggesting that the CO ligands are  $\mu^2$  and  $\mu^3$  bound. The shift in the  $\mu^3$  frequency toward higher frequencies could be explained by a lowered back-donation in the di-carbonyl complex. The whole band, which one could assume to consist of two overlapping bands for  $\mu^2$  and  $\mu^3$  bound CO in  $\text{Rh}_4(\text{CO})_2^+$ , shifts even more

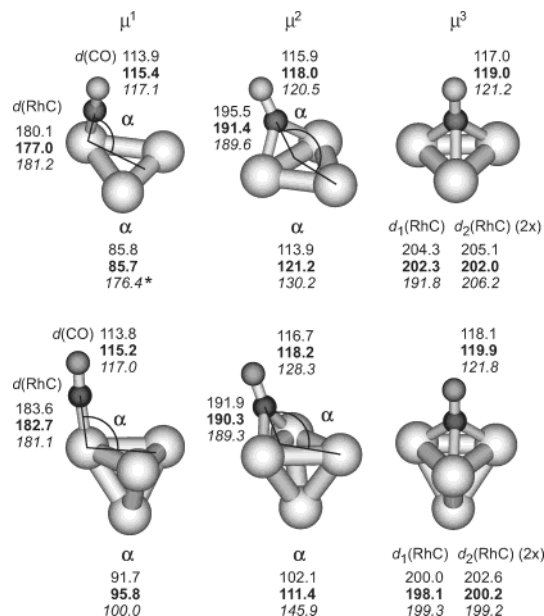


**Figure 6.** Optimized structures for  $\text{Rh}_n\text{CO}^{+/0/-}$  ( $n = 3$  and  $4$ ) complexes. The plotted structures correspond to the neutral species. Geometric parameters are given only for the CO and Rh–C bonds. The values of the geometric parameters are given for the cationic (plain font style), neutral (bold), and anionic (italic) complexes. In the  $\mu^1$  isomer,  $\alpha$  is the angle between the plane of three Rh atoms and the Rh–C bond and in the  $\mu^2$  isomer,  $\alpha$  is the angle between the plane of three Rh atoms and the plane through the Rh–C–Rh bonds. All distances are given in pm and the angles are in degrees. In anionic  $\mu^1$   $\text{Rh}_3\text{CO}^-$ , the CO is nearly in the plane of the Rh atoms, and the Rh–C–Rh angle is  $100.6^\circ$ .

to the blue by addition of a third CO molecule. We do not observe a splitting for the  $\mu^2$  and  $\mu^3$  bands, and therefore, this assignment is not fully conclusive; a rearrangement of the initial  $\mu^3$  complex by addition of the second CO and formation of a double  $\mu^2$  structure or involving a structure intermediate between  $\mu^2$  and  $\mu^3$  would be a possible alternative interpretation. In the spectrum of the tri-carbonyl species, an additional peak at  $2080 \text{ cm}^{-1}$  is observed indicating that bridging and atop sites are occupied in  $\text{Rh}_4(\text{CO})_3^+$ .

**DFT Calculations.** The results of our calculations on  $\text{Rh}_n\text{CO}^{+/0/-}$  ( $n = 3$  and  $4$ ) are summarized in Table 4 and Figure 6. The structures for isomers having the CO in atop ( $\mu^1$ ), bridging ( $\mu^2$ ), or a hollow site ( $\mu^3$ ) have been fully optimized without symmetry constraints.

To calculate the CO binding energies, the energetics of bare rhodium clusters have also been investigated. The ground states of the neutral and charged rhodium trimer all have triangular structures. The neutral trimer is an isosceles triangle ( $C_{2v}$ ) with sextet multiplicity and bond lengths of 250 pm ( $2\times$ ) and 247 pm. Its binding energy is 1.64 eV/atom. Above this ground-state, we find a doublet state and a quartet ( $C_{2v}$ ), 0.27 and 0.28 eV higher in energy. The ground state of  $\text{Rh}_3^+$  has been found to be a septet with  $C_s$  symmetry. The bond lengths are 256, 257, and 258 pm. The triplet ( $C_s$ ) and quintet ( $C_{2v}$ ) states are 0.09 and 0.33 eV higher in energy. For the anion  $\text{Rh}_3^-$ , we identify as a lowest state a quintet structure with  $C_{2v}$  symmetry and bond lengths of 250 pm ( $2\times$ ) and 259 pm. Singlet, triplet, and septet states are energetically very close but higher in energy by 0.12, 0.13, and 0.12 eV. The structures of  $\text{Rh}_4^{+/0/-}$  are all (distorted) tetrahedrons. For the bare  $\text{Rh}_4$  cluster, we find a  $T_d$  singlet ground state with a binding energy per atom of 1.95 eV and Rh–Rh distances of 247 pm, followed by a triplet state 0.12 eV higher in energy with  $D_{2d}$  symmetry. For the cationic

tetramer, we find the octet state ( $D_{2d}$  symmetry) to be the lowest with the doublet ( $C_{3v}$ ) and sextet ( $C_1$ ) isomers higher in energy by 0.40 and 0.45 eV, respectively. For the anion, the ground state is a sextet with the quartet state 0.27 eV and the doublet state 0.30 eV higher in energy (all have  $C_s$  symmetry). The adiabatic ionization potentials of  $Rh_3$  and  $Rh_4$  are calculated to be 6.88 and 6.03 eV and the electron affinities are 1.39 and 1.44 eV, respectively.

The identified ground state of the neutral  $Rh_4$  is in agreement with earlier calculations;<sup>17,25–27</sup> however, in these studies, several different ground states are suggested for  $Rh_3$  with multiplicities of 4 or 6. Experimentally, using electron spin resonance spectroscopy in a rare gas matrix, the trimer has been found to have a total spin of 5/2 and  $D_{3h}$  symmetry.<sup>28</sup> Raman spectroscopy identifies a  $C_{2v}$  structure; however, it is suggested that the barrier for pseudorotation might be very low.<sup>29</sup> To our knowledge, there is only one previous computational study on charged rhodium clusters.<sup>26</sup> For the ionic trimers, we identify the same ground state structures as given there, but for the charged tetramer, our results differ significantly, even if we consider only the three-dimensional  $Rh_4$  structures.

For the CO adducts on neutral and charged rhodium clusters, three different binding sites, atop ( $\mu^1$ ), bridging ( $\mu^2$ ), and a hollow site ( $\mu^3$ ) are considered. The calculated CO binding energies, frequencies, and IR intensities for the  $\nu(CO)$  and  $\nu(MC)$  stretch vibrations for the lowest energy  $\mu^1$ ,  $\mu^2$ , and  $\mu^3$  isomers of  $Rh_nCO^{+/0/-}$  ( $n = 3$  and  $4$ ) are listed in Table 4. Their geometries are shown in Figure 6. For  $Rh_3CO^{+/0/-}$ , the most strongly bound structure contains  $\mu^2$ -bridging CO. All of these structures have  $C_s$  symmetry and the CO bridge is bent out of the plane of the metal atoms. In the case of  $Rh_4CO$ , the relative energies clearly show that for the neutral and cationic species the CO on a  $\mu^3$  site is most stable. For the anion,  $\mu^1$  and  $\mu^3$  isomers are practically identical in energy. The  $\mu^3$  isomers have nearly  $C_{3v}$  symmetry, and in the  $\mu^2$  structures, the CO bridge is bent out of the facet plane similar as in the case of  $Rh_3CO^{+/0/-}$ . In the  $\mu^1$  structures, the CO is nearly perpendicular to one of the facets. This deviation from  $C_{3v}$  symmetry has been found already in the earliest calculations on  $Rh_4CO$  by Goursot et al.<sup>30</sup>

The values of  $\nu(CO)$  decrease as expected by  $\sim 100$   $cm^{-1}$  with increasing number of Rh atoms involved in the binding site between  $\mu^1$ ,  $\mu^2$ , and  $\mu^3$ . Increasing back-donation into the antibonding  $p_{\pi}^*$  CO orbitals when going from the cation over the neutral to the anion leads to successively decreasing  $\nu(CO)$  frequencies and increasing  $\nu(MC)$  stretch frequencies. The changes in the back-donation obviously also affect the IR intensities, leading to strong enhancement of the IR absorption cross section of the  $\nu(CO)$  mode.

Neutral  $Rh_4CO$  has been investigated in three earlier theoretical studies as a model for CO adsorption on a metal (111) surface or a deposited nanocluster. In the study of Goursot et al.,<sup>30</sup> the adsorption of CO on tetrahedral  $Rh_4$  is modeled yielding an energetical preference for  $\mu^1$  and  $\mu^2$  bound isomers that are close in energy. Blyholder<sup>31</sup> used a flat  $Rh_4$  cluster with  $\mu^1$  bound CO to model the presumed geometry of a deposited cluster. In both of these studies, the geometry of the metal cluster has not been relaxed. In the more recent study of Mineva et al.,<sup>32</sup> only  $\mu^1$  structures are considered for  $Rh_3CO$  and  $Rh_4CO$ . Our geometries and electronic ground states for neutral  $\mu^1$   $Rh_3CO$  and  $Rh_4CO$  are in agreement with the results of Mineva et al., although we find that these are not the most stable structures and they are not abundant in the experiment. The preference for modeling  $\mu^1$  structures is probably induced by IR absorption measurements on CO adsorbed on small deposited

clusters, where at low coverages actually mainly  $\mu^1$  bound CO is detected.<sup>3–5</sup> Majumdar and Balasubramanian have made a comprehensive study of  $Rh_3CO$  using a complete active space multi-configuration self-consistent field (CASMCSCF) method followed by multireference singles and doubles interaction (MRSDCI) that predicts a doublet ground state with CO  $\mu^3$  bound and  $\nu(CO) = 1907$   $cm^{-1}$ .<sup>33</sup> This is in disagreement with our DFT studies that find a quartet,  $\mu^3$  bound ground state for  $Rh_3CO$  with  $\nu(CO) = 1723$   $cm^{-1}$ . Although we do not have a value for  $\nu(CO)$  for neutral  $Rh_3CO$  for direct comparison with theory, the consistent agreement between DFT theory and experiment for  $Rh_3CO^+$  and  $Rh_4CO^{-/0/+}$  supports our DFT result for  $Rh_3CO$ .

The structural assignments for  $Rh_3CO^+$  and  $Rh_4CO^{+/0/-}$  based on the IR-MPD spectra agree with the energetically lowest structures obtained in the DFT calculations. A special case is only  $Rh_4CO^-$ , for which the DFT calculations find  $\mu^1$  and  $\mu^3$  to be isoenergetic, whereas the IR-MPD spectra only show evidence for  $\mu^1$  binding. For  $Rh_3CO^+$ , the agreement between experiment and theory is exceptionally good, whereas for the  $Rh_4CO^{+/0/-}$  complexes, the experimental frequencies are reproduced less well by the calculations. Especially, the experimental  $\nu(CO)$  frequency for neutral  $Rh_4CO$  lies between the calculated values for the  $\mu^2$  and  $\mu^3$  isomer. Nonetheless, the position of the  $\nu(CO)$  band relative to the  $\mu^1$  and  $\mu^2$  bands of the larger cluster complexes allows us to assign the present species to be  $\mu^3$  bound CO.

#### Implications for Charge Transfer in Supported Clusters.

Our results on gas phase rhodium cluster complexes can be compared to data obtained for clusters of similar size that are deposited on a substrate. In making this comparison, one must be aware that the situation of a cluster on a surface is far more complex than in the gas phase. Gas phase structures may not be maintained on the surface, their symmetries are reduced, the surface may sterically hinder CO adsorption, and charge distributions in the cluster may be different due to site-specific cluster surface interactions. Nevertheless, the gas-phase measurements form a baseline to gauge the surface induced perturbations and the comparison is important.

There are two recent reports of  $\nu(CO)$  for CO adsorbed on supported clusters of known size. Mono-carbonyl complexes of Rh nanoparticles with an average size of five to six atoms (determined by STM) on highly ordered  $Al_2O_3$  films have  $\nu(CO)$  reported at 2000 and 1966  $cm^{-1}$ .<sup>5</sup> In this size range, we find  $\nu(CO)_{neutral}$  in the range of 1949–1960  $cm^{-1}$  and  $\nu(CO)_{cation}$  in the range of 2038–2054  $cm^{-1}$  for isolated complexes (Table 3). The dependence of  $\nu(CO)$  on the cluster charge is plotted in Figure 7. From this plot, we can estimate the charge on the supported clusters with  $\nu(CO)$  at 2000  $cm^{-1}$  to be in the range of +0.4 to +0.6 e. A possible explanation for the second peak reported in ref 5 could be the presence of a second adsorption site for the clusters on the  $Al_2O_3$  substrate where charge transfer is minimal, resulting in  $\nu(CO) = 1966$   $cm^{-1}$ . For comparison, similar arguments based on matrix values of  $\nu(CO)$  for  $RhCO^{+/0}$  put the charge on the atom complex,  $RhCO$ , adsorbed at oxide line defects on the same films at +0.6 e to +0.7 e.<sup>5</sup> In work on CO adsorbed on size-selected  $Rh_8$  deposited on  $MgO(100)$  films  $\nu(CO)$  is reported at 2066  $cm^{-1}$ .<sup>2</sup> This is 40  $cm^{-1}$  higher than the value we find for the free cation,  $Rh_8CO^+$ . In the deposition experiments, the number of CO ligands adsorbed to  $Rh_8$  is not determined, and it is likely that more than one CO ligand is adsorbed. We observe that binding of up to three CO ligands to the free clusters induces only small shifts to the blue. The apparent implication is that the charge on the deposited cluster

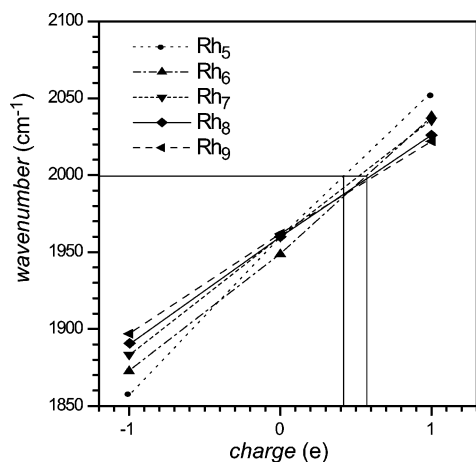


**Figure 7.** Dependence of the position of the  $\mu^1 \nu(\text{CO})$  band on the cluster charge for clusters of 5–9 atoms. The horizontal line indicates the  $\nu(\text{CO})$  value of  $2000 \text{ cm}^{-1}$  that is measured for CO on deposited Rh clusters of similar size.<sup>5</sup> From the points of intersection with the connection lines between the gas phase  $\nu(\text{CO})$  values we estimate the partial charges on the deposited Rh<sub>5</sub> and Rh<sub>6</sub> cluster.

may be greater than +1 e; however, it can also not be excluded that the cluster does not remain intact as Rh<sub>8</sub> following either deposition or reaction with CO. Also the formation of geminal carbonyls may play a role at high CO coverage of the surface. Those species would exhibit further blue-shifted  $\nu(\text{CO})$  bands as for example in Rh<sub>4</sub>CO<sub>12</sub> or Rh<sub>6</sub>CO<sub>16</sub>. For CO adsorbates on a technical catalyst, Rh/Al<sub>2</sub>O<sub>3</sub>, both  $\mu^1$  adsorption sites, with  $\nu(\text{CO})$  in the range 2042–2076  $\text{cm}^{-1}$ , and  $\mu^2$  sites, with  $\nu(\text{CO})$  in the range 1845–1875  $\text{cm}^{-1}$ , have been identified.<sup>34</sup> These values are consistent with our measurements on free clusters provided that the clusters formed by the reduction of rhodium salts on Al<sub>2</sub>O<sub>3</sub> are relatively small ( $n < 5$ ) and carry a significant positive charge.

## V. Conclusion: Size and Charge Effects

From our IR spectra reported here, a general picture of the binding of CO to gas-phase Rh clusters emerges. We find two different regimes of CO binding depending on the cluster size. Clusters with  $n \geq 5$  show predominantly  $\mu^1$  binding, independent of charge state. In some selected cases,  $\mu^2$  binding is observed in addition to  $\mu^1$  binding. This formation of isomeric complexes can be attributed to Rh<sub>n</sub> cluster isomers or to the presence of different, nearly isoenergetic binding sites on the clusters. The propensity to form isomers with  $\mu^2$  bridge binding increases with electron density on the cluster. As the cluster size increases, one expects the properties of the charged species to converge to those of the neutral species and eventually to those of bulk material. For the  $\nu(\text{CO})$  values, this point has not been reached at  $n = 15$ . Studies of larger clusters and a detailed discussion of the charge-induced effects in larger clusters are underway.

The smaller clusters with  $n \leq 4$  show a much more dramatic dependence of the nature of the binding site with both size and charge. Our experimental IR spectra show that in cationic and neutral Rh<sub>4</sub>CO<sup>+0</sup> CO is bridge bound at a 3-fold hollow site, whereas in the anion, it is atop bound. In Rh<sub>3</sub>CO<sup>+</sup>, CO is bound at a 2-fold bridging site. This is in agreement with results from our DFT calculations.

In conclusion, we have demonstrated that IR-MPD can be used to probe the structure of adsorbates on gas phase metal clusters. For the adsorption of CO on Rh clusters, the adsorption sites strongly depend on the cluster size and on the charge of the cluster. This new possibility to get insights into the structural properties of cluster adsorbates holds great promise for the

development of a chemically intuitive understanding of the chemistry of small metal clusters.

**Acknowledgment.** We gratefully acknowledge the support of the Stichting voor Fundamenteel Onderzoek der Materie (FOM) in providing beam time on FELIX and the skill of the FELIX staff, in particular Dr. A. F. G. van der Meer and Dr. B. Redlich. A.F. acknowledges financial support by the European Union IHP Research Training Network “Delayed Ionization and Competing Cooling Mechanisms in Atomic Clusters”.

## References and Notes

- (1) Yates, J. T., Jr.; Duncan, T. M.; Worley, S. D.; Vaughan, R. W. *J. Chem. Phys.* **1979**, *70*, 1219–1224.
- (2) Heiz, U.; Sanchez, A.; Abbet, S.; Schneider, W.-D. *Chem. Phys.* **2000**, *262*, 189–200.
- (3) Frank, M.; Kühnemuth, R.; Bäumer, M.; Freund, H.-J. *Surf. Sci.* **1999**, *427–428*, 288–293.
- (4) Frank, M.; Kühnemuth, R.; Bäumer, M.; Freund, H.-J. *Surf. Sci.* **2000**, *454–456*, 968–973.
- (5) Frank, M.; Bäumer, M.; Kühnemuth, R.; Freund, H.-J. *J. Phys. Chem. B* **2001**, *105*, 8569–8576.
- (6) Zhou, M.; Andrews, L. *J. Phys. Chem. A* **1999**, *103*, 7773–7784.
- (7) Zhou, M.; Andrews, L. *J. Am. Chem. Soc.* **1999**, *121*, 9171–9175.
- (8) Simard, B.; Dénommée, S.; Rayner, D. M.; van Heijnsbergen, D.; Meijer, G.; von Helden, G. *Chem. Phys. Lett.* **2002**, *357*, 195–203.
- (9) Fielicke, A.; von Helden, G.; Meijer, G.; Simard, B.; Dénommée, S.; Rayner, D. M. *J. Am. Chem. Soc.* **2003**, *125*, 11184–11185.
- (10) Oepts, D.; van der Meer, A. F. G.; van Amersfoort, P. W. *Infrared Phys. Technol.* **1995**, *36*, 297–308.
- (11) von Helden, G.; van Heijnsbergen, D.; Meijer, G. *J. Phys. Chem. A* **2003**, *107*, 1671–1688.
- (12) Fielicke, A.; Meijer, G.; von Helden, G. *J. Am. Chem. Soc.* **2003**, *125*, 3659–3667.
- (13) Collings, B. A.; Amrein, A. H.; Rayner, D. M.; Hackett, P. A. *J. Chem. Phys.* **1993**, *99*, 4174–4180.
- (14) Yang, D.-S.; Zgierski, M. Z.; Rayner, D. M.; Hackett, P. A.; Martinez, A.; Salahub, D. R.; Roy, P.-N.; Tucker Carrington, J. *J. Chem. Phys.* **1995**, *103*, 5335–42.
- (15) Bechthold, P. S.; Parks, E. K.; Weiller, B. H.; Pobo, L. G.; Riley, S. J. *J. Phys. Chem. NF* **1990**, *169*, 101–122.
- (16) Jaguar 4.0; Schrödinger Inc.: Portland, OR, 1991–2000.
- (17) Mainardi, D. S.; Balbuena, P. B. *J. Phys. Chem. A* **2003**, *107*, 10370–10380.
- (18) Krishnan, R.; Binkley, J. S.; Seeger, R.; Pople, J. A. *J. Chem. Phys.* **1980**, *72*, 650–654.
- (19) Hay, P. J.; Wadt, W. R. *J. Chem. Phys.* **1985**, *82*, 270–83.
- (20) Balteanu, I.; Achatz, U.; Balaj, O. P.; Fox, B. S.; Beyer, M. K.; Bondybeg, V. E. *Int. J. Mass Spectrom.* **2003**, *229*, 61–65.
- (21) Knickelbein, M. B.; Yang, S. J. *J. Chem. Phys.* **1990**, *93*, 5760–67.
- (22) Athanassenas, K.; Kreisle, D.; Collings, B. A.; Rayner, D. M.; Hackett, P. A. *Chem. Phys. Lett.* **1993**, *213*, 105–110.
- (23) Beck, W.; Lottes, K. *Chem. Ber.* **1961**, *94*, 2578–2582.
- (24) Corey, E. R.; Dahl, L. F.; Beck, W. *J. Am. Chem. Soc.* **1963**, *85*, 1202–1203.
- (25) Chien, C.-H.; Blaisten-Barojas, E.; Pederson, M. R. *Phys. Rev. A* **1998**, *58*, 2196–2202.
- (26) Lacaze-Dufour, C.; Mineva, T.; Russo, N. *Int. J. Quantum Chem.* **2001**, *85*, 162–170.
- (27) Wang, L.; Ge, Q. *Chem. Phys. Lett.* **2002**, *366*, 368–376.
- (28) Van Zee, R. J.; Hamrick, Y. M.; Li, S.; Weltner, W., Jr. *Chem. Phys. Lett.* **1992**, *195*, 214–220.
- (29) Fang, L.; Shen, X.; Chen, X.; Lombardi, J. R. *J. Chem. Phys.* **2000**, *113*, 7178–7181.
- (30) Goursot, A.; Papai, I.; Salahub, D. R. *J. Am. Chem. Soc.* **1992**, *114*, 7452–7458.
- (31) Blyholder, G. *J. Mol. Catal. A* **1997**, *119*, 11–17.
- (32) Mineva, T.; Russo, N.; Freund, H.-J. *J. Phys. Chem. A* **2001**, *105*, 10723–10730.
- (33) Majumdar, D.; Balasubramanian, K. *J. Chem. Phys.* **1997**, *106*, 7215–7222.
- (34) Rice, C. A.; Worley, S. D.; Curtis, C. W.; Guin, J. A.; Tarrer, A. R. *J. Chem. Phys.* **1981**, *74*, 6487–6497.
- (35) Callender, C. L.; Hackett, P. A.; Rayner, D. M. *J. Opt. Soc. Am. B* **1988**, *5*, 614–618.
- (36) Moore, C. E. *Atomic Energy Levels*; Circ. 467; National Bureau of Standards (U. S.): Gaithersburg, MD, 1958; Vol. III.
- (37) Scheer, M.; Brodie, C. A.; Bilodeau, R. C.; Haugen, H. K. *Phys. Rev. A* **1998**, *58*, 2051–2062.